Check for updates

Bioelectromagnetics 39:631–643 (2018)

# Effect of Low-Level 1800 MHz Radiofrequency Radiation on the Rat Sciatic Nerve and the Protective Role of Paricalcitol

**Ulku Comelekoglu,[1] Savas Aktas,[2]* Burcu Demirbag,[2] Meryem Ilkay Karagul,[2] Serap Yalin,[3] Metin Yildirim,[3] Aysegul Akar,[4] Begum Korunur Engiz,[5] Fatma Sogut,[6] and Erkan Ozbay[1]**

[1]*Faculty of Medicine, Department of Biophysics, Mersin University, Mersin, Turkey*
[2]*Faculty of Medicine, Department of Histology and Embryology, Mersin University, Mersin, Turkey*
[3]*Faculty of Pharmacy, Department of Biochemistry, Mersin University, Mersin, Turkey*
[4]*Faculty of Medicine, Department of Biophysics, Ondokuz Mayıs University, Samsun, Turkey*
[5]*Faculty of Engineering, Department of Electrical and Electronics Engineering, Ondokuz Mayıs University, Samsun, Turkey*
[6]*Vocational School of Medical Services, Department of Perfusion, Mersin University, Mersin, Turkey*

The nervous system is an important target of radiofrequency (RF) radiation exposure since it is the excitable component that is potentially able to interact with electromagnetic fields. The present study was designed to investigate the effects of 1,800 MHz RF radiation and the protective role of paricalcitol on the rat sciatic nerve. Rats were divided into four groups as control, paricalcitol, RF, and RF + paricalcitol. In RF groups, the rats were exposed to 1,800 MHz RF for 1 h per day for 4 weeks. Control and paricalcitol rats were kept under the same conditions without RF application. In paricalcitol groups, the rats were given 0.2 μg/kg/day paricalcitol, three times per week for 4 weeks. Amplitude and latency of nerve compound action potentials, catalase activities, malondialdehyde (MDA) levels, and ultrastructural changes of sciatic nerve were evaluated. In the RF group, a significant reduction in amplitude, prolongation in latency, an increase in the MDA level, and an increase in catalase activity and degeneration in the myelinated nerve fibers were observed. The electrophysiological and histological findings were consistent with neuropathy, and the neuropathic changes were partially ameliorated with paricalcitol administration. Bioelectromagnetics. 39:631–643, 2018. © 2018 Wiley Periodicals, Inc.

**Keywords: radiofrequency radiation; 1800 MHz; sciatic nerve; oxidative stress; paricalcitol**

## INTRODUCTION

Mobile phones and other wireless communication devices are used widely in the modern world. Mobile phones emit radiofrequency (RF) radiation ranging from 900 to 1,800 MHz. The widespread use of mobile phones poses the problem of possible health effects on many physiological functions such as memory impairment [Kalafatakis et al., 2017], increase in parasympathetic nerve activity [Misek et al., 2018], increase in thyroid function [Baby et al., 2017], weakening of the immune system [El-Gohary and Said, 2017], and increase in the permeability of blood-brain barrier [Sırav and Seyhan, 2016].

The effects of 900–1,800 MHz RF on the nervous system have been investigated in different studies. In these studies, it was shown that exposure to RF radiation may cause changes in amygdala morphology and emotional behavior [Narayanan et al., 2018] and changes in cerebral cortex neurotransmitter release [Kim et al., 2017]. In addition, it has been reported that RF radiation may lead to cytotoxicity in

Conflict of Interest: None

*Correspondence to: Savas Aktas, Department of Histology and Embryology, Faculty of Medicine, Mersin University, 33342 Mersin, Turkey. E-mail: saktas@mersin.edu.tr

Received for review 17 May 2018; Accepted 26 September 2018

DOI: 10.1002/bem.22149
Published online 16 October 2018 in Wiley Online Library (wileyonlinelibrary.com).

© 2018 Wiley Periodicals, Inc.

hippocampal neuronal HT22 cells [Kim et al., 2017] and degenerative changes in hippocampus pyramidal cells [Hussein et al., 2016]. In a recent study, evidence was provided showing an association between mobile phone use and brain tumors, especially in people who used their mobile phones for more than 10 years [Prasad et al., 2017]. In another study, it was reported that long-term use of mobile phones was linked to an increased risk of intracranial tumors [Bortkiewicz et al., 2017]. These studies show that the nervous systems of both humans and animals are sensitive to RF. However, there are studies in the literature that suggest that exposure to RF radiation does not cause any adverse health effects [Chapman et al., 2016; Mohan et al., 2016; Sato et al., 2017].

Action potentials are of great importance to the functioning of the nervous system since they propagate information from the periphery nervous system to the central nervous system and propagate commands initiated in the central nervous system to the periphery nervous system. Measurements of action potential depolarization and repolarization phases may provide information about the behavior of $Na^+$ and $K^+$ ions [Aminoff, 1998]. In addition, action potential parameters such as amplitude and latency detect chronic axonal loss and demyelination in the nerve fiber, respectively.

Oxidative stress plays a role in the development of a number of nervous system disorders [Niedzielska et al., 2016]. Oxygen is vital but potentially dangerous and there is a complex system of controls and balances to use this basic element. Oxidative stress is a consequence of the imbalance of pro-oxidant/antioxidant homeostasis, which leads to the formation of toxic reactive oxygen species (ROS) [Niedzielska et al., 2016]. Recent studies have shown that cell phone radiation increases oxidative stress [Grundler et al., 1992; Oktem et al., 2005; Oral et al., 2006; Ozguner et al., 2006; Balci et al., 2007; Meral et al., 2007; Dasdag et al., 2008; Xu et al., 2010]. Also, there are some studies on the use of pulsed RF currents in the treatment of chronic pain and arthroscopic surgery [Hagiwara et al., 2009; Chua et al., 2011; Martin et al., 2014].

Paricalcitol (19-nor-1α,25-dihydroxyvitamin $D_2$) is a newly developed analog of $1,25(OH)_2D_3$ that has minimal effects on calcium and phosphorus levels. Paricalcitol has shown some promise regarding redox homeostasis in preclinical studies [Husain et al., 2009; Husain et al., 2010].

As can be seen from the literature review, studies on the effects of RF radiation on the nervous system are more focused on the central nervous system. There are a limited number of studies that have investigated the effect of RF radiation on peripheral nerves [Acar et al., 2009; Yegin et al., 2017; Kerimoğlu et al., 2018]. Therefore, the present study aimed to investigate the effects of 1800 MHz global system for mobile communications (GSM)-like RF radiation (average E-field $6.05 \pm 0.67$ V/m, whole-body average specific absorption rate (SAR) value: 0.00421W/kg, in 10 g tissue) on rat sciatic nerve, as well as the possible protective effect of paricalcitol. To the best of our knowledge, the present study seems to be the first investigation in the literature focusing on the electrophysiological, biochemical, and histological effects of 1800 MHz GSM-like low-level RF radiation and paricalcitol on the sciatic nerve.

## MATERIALS AND METHODS

### Animals

Twenty-eight healthy adult male Wistar albino rats (mean body mass $192.5 \pm 18.7$ g) were used in this study. Rats were obtained from the Experimental Animal Center, University of Mersin (Mersin, Turkey). The study was approved by the Local Ethics Committee for Experimental Animals at the University of Mersin. The rats were housed in polycarbonate cages (7 rats per cage) at $22 \pm 1.5$ °C and 55% humidity level under the 12:12 h day–night cycle. Rats were fed with standard pelleted food and were given water ad libitum. The rats were randomly assigned into four groups, each consisting of 7 rats: the control, paricalcitol (0.2 μg/kg/day paricalcitol, three times per week for 4 weeks), RF (1,800 MHz EMF for 1 h, through 4 weeks), and RF + paricalcitol groups (1,800 MHz EMF for 1 h, through 4 weeks and 0.2 μg/kg/day paricalcitol, three times per week for 4 weeks). During the study, the control and paricalcitol rats were made to stay in the restrainer for 1 h/day without being exposed to RF radiation in order to eliminate the stress factor. All experiments were performed in accordance with the National Institutes of Health's Guide for the Care and Use of Laboratory Animals.

### Exposure System

In this study, a continuous RF radiation at 1,800 MHz was used. RF simulator (1800CW2, Everest, Adapazari, Turkey) emitting continuous or intermittent wave in 217 Hz modulation had 2 W maximum output power, 2 RF outputting channel, and a monopole antenna (Everest, Adapazari, Turkey). A galvanized plate was placed under a pie cage restrained to decrease magnetic field effect and static



1521186x, 2018, 8, Downloaded from https://onlinelibrary.wiley.com/doi/10.1002/bem.22149 by University Of British Columbia, Wiley Online Library on [16/10/2026]. See the Terms and Conditions (https://onlinelibrary.wiley.com/terms-and-conditions) on Wiley Online Library for rules of use; OA articles are governed by the applicable Creative Commons License

electric field effects. Prior to the study, electrical and magnetic fields in the laboratory were measured in order to check the background of electromagnetic sources. A portable electric field meter (PMM 8053, Elettroniche CentroMisure Radioelettriche, Savano, Italy) was used to measure the electric field, and digital Gauss/Tesla meter (Sypris 6010, F.W. Bell, San Diego, CA) was used to measure the magnetic field. The exposure design of rats is given in Figure 1. Here, a galvanized plate was placed under the pie cage restrained to decrease magnetic field effect and static electric field effects. To achieve uniform dispersion of the electrical field to rats, the antenna, which is a height of approximately 15 cm from the bottom of galvanized plate, was located in the center of the pie cage restrainer ($42 \times 20 \times 7$ cm) consisting of 12 slices in vertical position. To reduce stress on the treatment group rats, a series of air holes about 1 cm diameter were formed in the upper surface of the pie cage restrainer. The coaxial cable-rat distance in the horizontal position was about 9 cm. Due to the movement of the rats, the coaxial cable-rat distances varied between 7 and 10 cm during exposure.

### E-Field Measurement and SAR Calculation

The accuracy of the produced 1,750–1,850 MHz band interval frequencies was checked by a Prolink-4C Premium model spectrum analyzer (Promax MC-877C, Barcelona, Spain). In the experiment, each rat in the RF and RF + paricalcitol groups was put into the pie cage restrainer and output power of the generator was fixed at 0.2 W. Restraining of the animals may increase exposure homogeneity [Allen et al., 2009]. The rats were exposed to RF radiation for 1 h at the same time every day for 30 consecutive days. During the study, the control and paricalcitol rats were made to stay in the restrainer for 1 h/day without being exposed to RF radiation in the same conditions. For use in dosimetric evaluation, at the first week of the study and at the last week of the study, E-field measurements were taken from the head, dorsal, and tail regions of rats for 2 min with portable field meter on different places of the rats in the 12-slice rat restrainer during the RF application. A whole-body average E-field value was calculated from these electric field values. Average E-field was $6.05 \pm 0.67$ V/m. This measured E-field value was used in an electromagnetic field solver to find the electric field distribution and to calculate SAR. Dosimetry plays an important role in risk evaluation of human exposure to RF fields, for example, evaluation of SAR.

In vivo measurement of electromagnetic field distribution inside the body is commonly not possible. Therefore, numerical field computations based on volume discretization schemes such as the Finite Differences method, the Finite Element method, or the Finite Integration Technique (FIT) often use high-resolution models based on volume pixel [Clemens et al., 2009].

In the present study, a commercial software package, the Transient Solver within CST Microwave Studio 2018 (Computer Simulation Technology, Darmstadt, Germany), was used to solve the electric field distribution and evaluate SAR. This provided a solution to time-dependent Maxwell's equations using a time-domain variant of the FIT. The voxel (volumetric pixel) rat model was created using computerized tomography scans of a rat that were obtained from CST, and this model was used in field simulations. The experimental setup that consisted of rat models and a λ/2 monopole antenna was modeled using CST

Fig. 1. RF exposure system.



1521186x, 2018, 8, Downloaded from https://onlinelibrary.wiley.com/doi/10.1002/bem.22149 by University Of British Columbia, Wiley Online Library on [16/10/2026]. See the Terms and Conditions (https://onlinelibrary.wiley.com/terms-and-conditions) on Wiley Online Library for rules of use; OA articles are governed by the applicable Creative Commons License

Studio Suite to determine the distribution of E (electric field strength) and SAR. Perfect boundary approximation was used for spatial discretization. Hexahedral mesh type was used, and the mesh was produced by an automatic mesh generator in order to ensure a good compromise between accuracy and simulation time. IEEE/IEC 62704-1 averaging method was used to determine the peak spatial-average SAR in the rat voxel model whose 10 g of averaging mass was exposed to RF.

### Recordings of Compound Motor Action Potentials (CMAP)

All electrophysiological experiments were done under general anesthesia. The rats were anesthetized with ketamine-HCl (90 mg/kg) and xylazine (10 mg/kg) (Eczacıbaşı İlaç Sanayi, Istanbul, Turkey). CMAP was recorded in all groups using standardized nerve conduction study techniques [Aminoff, 1998]. Data were collected by electrophysiological recording station (MP 100 acquisition system, BIOPAC Systems, Santa Barbara, CA). A bipolar stimulating electrode was placed on the sciatic notch. CMAP recordings were done with Ag–AgCl disc electrodes (BIOPAC Systems). The cathode was placed over the belly of gastrocnemius muscle at the midline while anode was over the tendon of the same muscle. The ground electrode was placed on the thigh on the side of stimulation (Fig. 2). Filter setting was 2–10 kHz for recordings. The supramaximal stimulus consisted of a single square pulse (intensity 5V, duration 0.5 ms). CMAP was previously raised on the amplifiers and then transferred to computers that translated to numerical signals by 16 bit A/D converter for offline analysis. The sampling rate was chosen as 20,000 sample/s. In all groups, the point of stimulation was kept constant. Latency and amplitude were measured from CMAP recordings. Latency is the time in milliseconds from the stimulus artifact to the first negative deflection of CMAP. It is the measure of conduction in the fastest conducting motor nerve fibers. The amplitude of CMAP was measured from the baseline to the negative peak (base to peak). AcqKnowledge analysis software (BIOPAC Systems) was used to measure CMAP latency and amplitude.

### Biochemical Evaluation

Sciatic nerve samples were homogenized (T 25 Ultra-Turrax, IKA-Werke, Staufen, Germany) with 50 mM phosphate buffered saline (PBS) (pH 7,4) (Sigma–Aldrich, St Louis, MO). Then, homogenates were centrifuged (Mikro 22R, Hettich, Tuttlingen, Germany) at 10,000*g* for 15 min at 4 °C. Supernatants were separated and kept at 20 °C until enzyme activities and malondialdehyde (MDA) measurements were performed. Protein in supernatants was determined as described before, using bovine serum albumin as standard [Lowry et al., 1951]. Tissue

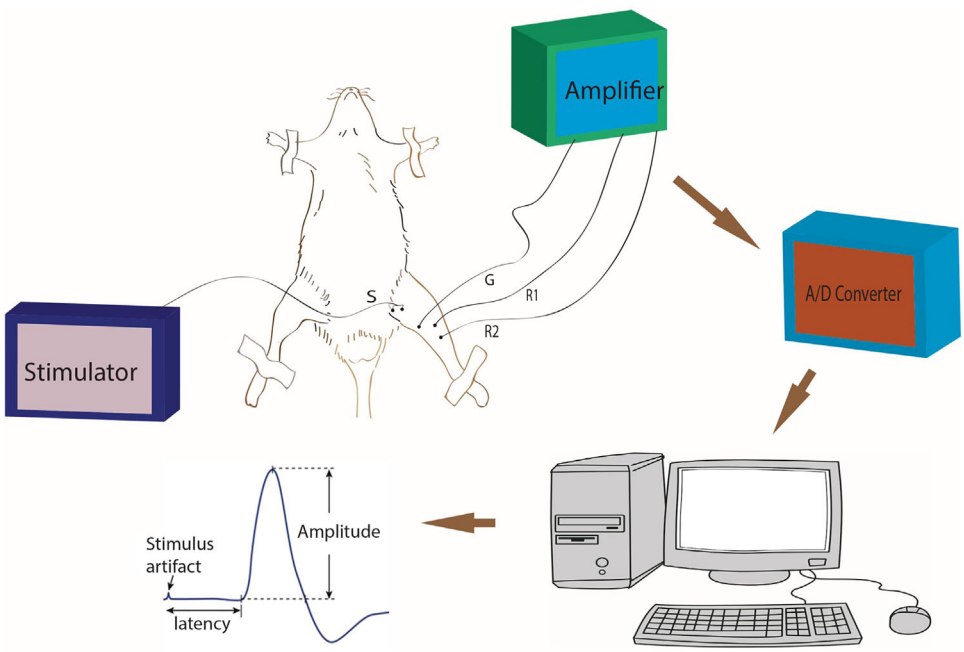


Fig. 2. Experimental setup for CMAP recordings. S: bipolar stimulating electrode, G: ground electrode, R1 cathode of recording electrode, R2 anode of recording electrode.



1521186x, 2018, 8, Downloaded from https://onlinelibrary.wiley.com/doi/10.1002/bem.22149 by University Of British Columbia, Wiley Online Library on [16/10/2026]. See the Terms and Conditions (https://onlinelibrary.wiley.com/terms-and-conditions) on Wiley Online Library for rules of use; OA articles are governed by the applicable Creative Commons License

MDA levels, an index of lipid peroxidation, were determined by thiobarbituric acid (TBA) reaction. The color complexes produced by the interaction of TBA (Sigma–Aldrich Chemical, St. Louis, MO) with MDA were measured at 532 nm on a spectrophotometer (Varian, Palo Alto, CA). The colored reaction with 1,1,3,3-tetraethoxypropane (Sigma–Aldrich Chemical) was used as the primary standard. MDA levels were determined by a previously defined method of Yagi [1998]. MDA levels were expressed as nanomoles per milligram of protein (nmol/mg protein). Tissue catalase (CAT) activity was measured in supernatants by the method of Aebi [1984]. Decomposition of the substrate $H_2O_2$ was monitored spectrophotometrically at 240 nm. Specific activity was defined as micromole substrate decomposed per min per milligram of protein (U/mg protein).

### Histological Methods

Sciatic nerve tissues were fixed in 2.5% glutaraldehyde (Electron Microscopy Sciences, Fort Washington, PA). After fixation, tissues were postfixed in 1% osmium tetroxide (Electron Microscopy Sciences) and processed routinely for electron microscopy and embedded in resin kit (Electron Microscopy Sciences). Semi-thin sections (1 μm) and ultra-thin sections (50–70 nm) were cut with an ultramicrotome (UCT-125, Leica Microsystems, Wien, Austria). Semi-thin sections were stained with toluidine blue and were examined with a light microscope (BX50, Olympus, Tokyo, Japan) and photographed with a digital camera system (LC30, Olympus, Tokyo, Japan) attached to the microscope.

For myelin sheath thickness and g-ratio (axon diameter/fiber diameter), at least 1000 myelinated nerve fibers of each animal were assessed. Four digital images (total area: $672 \times 612$ μm) per sciatic nerve were photographed with an X40 objective. Digital images were analyzed on a PC with image analysis software (iTEM 5.0, Olympus Soft Imaging Solutions, Münster, Germany).

Ultra-thin sections were contrasted with uranyl acetate-lead citrate and were examined with an electron microscope (JEM 1011, Jeol, Tokyo, Japan) and were photographed with a digital camera (Megaview III, Olympus Soft Imaging Solutions) attached to the microscope. For ultrastructural evaluation of myelin sheath damage (Table 1) [Kaptanoglu et al., 2002] and axonal damage (Table 2) [Erdine et al., 2009], a semi-quantitative evaluating method was used. Fifty myelinated nerve fibers from each sample and a total of 350 myelinated fibers from each group were evaluated ultrastructurally.

**TABLE 1. Ultrastructural Grading System of Myelinated Axons**

| | |
|---|---|
| Grade 0 | Normal |
| Grade 1 | Separation in myelin configuration |
| Grade 2 | Interruption in myelin configuration |
| Grade 3 | Honeycomb appearance |
| Grade 4 | Collapsed myelin forming ovoids |

### Statistical Analysis

Data were analyzed using a statistical package program (v.11.5, SPSS, Chicago, IL). The checks of normality of variables were tested with Kolmogorov–Smirnov test. Descriptive statistics of variables were expressed as mean ± standard deviation. The differences between the groups were tested by analysis of variance (one-way ANOVA) for the data showing normal distribution. Tukey test was used for multiple comparison tests. $P$ values less than 0.05 were considered as statistically significant.

## RESULTS

### Distribution of E Field and SAR

The distribution of E field and SAR are given in Figure 3A and 3B, respectively. As seen from Figure 3B, the maximum SAR (10 g) is 0.00421 W/kg.

### Electrophysiological Findings

One recording sample for all groups is given in Figure 4. As seen from the recordings, the RF radiation reduced the amplitude of CMAP in RF group. Values of mean CMAP amplitude were

**TABLE 2. Scoring of Damage to Axonal Ultrastructure**

| Score | Degree of damage | Description of damage |
|---|---|---|
| 1− | No damage | Mitochondria, microtubules, and microfilaments normal |
| 1+ | Low damage | Some vacuole and inclusions, some swelling in the mitochondria; and microtubule and microfilaments normal |
| 2+ | Mild damage | Large vacuoles, damaged external membrane and crista, formation of multilaminar structures, and swollen shape of mitochondria; and occasional abnormalities on the microtubules and microfilaments |
| 3+ | High damage | The same as in 2+ (mild damage), but in addition large areas of fragmented microtubules and microfilaments, or substantial absence of microtubules |



1521186x, 2018, 8, Downloaded from https://onlinelibrary.wiley.com/doi/10.1002/bem.22149 by University Of British Columbia, Wiley Online Library on [16/10/2026]. See the Terms and Conditions (https://onlinelibrary.wiley.com/terms-and-conditions) on Wiley Online Library for rules of use; OA articles are governed by the applicable Creative Commons License

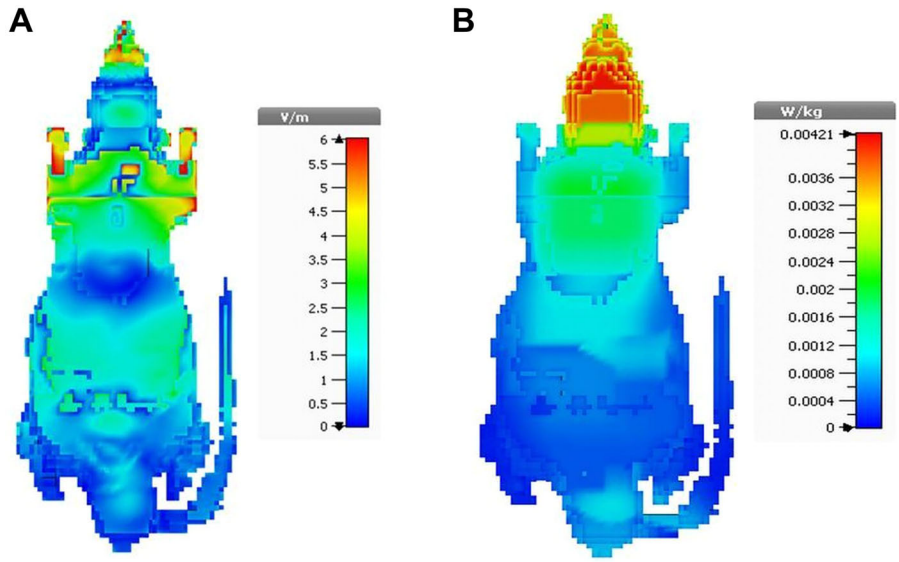


Fig. 3. Electric field distribution on voxel rat model (A) and SAR over 10 grams of tissue for the voxel rat model (B).

$8.25 \pm 0.57$, $7.09 \pm 0.60$, $2.39 \pm 0.67$, and $5.64 \pm 0.78$ mV in control, paricalcitol, RF, and RF + paricalcitol groups, respectively. RF radiation of 1,800 MHz significantly reduced the nerve action potential amplitude compared to the control, paricalcitol, and RF + paricalcitol values ($P < 0.05$). There was no significant difference between the control group and paricalcitol group. In the RF + paricalcitol

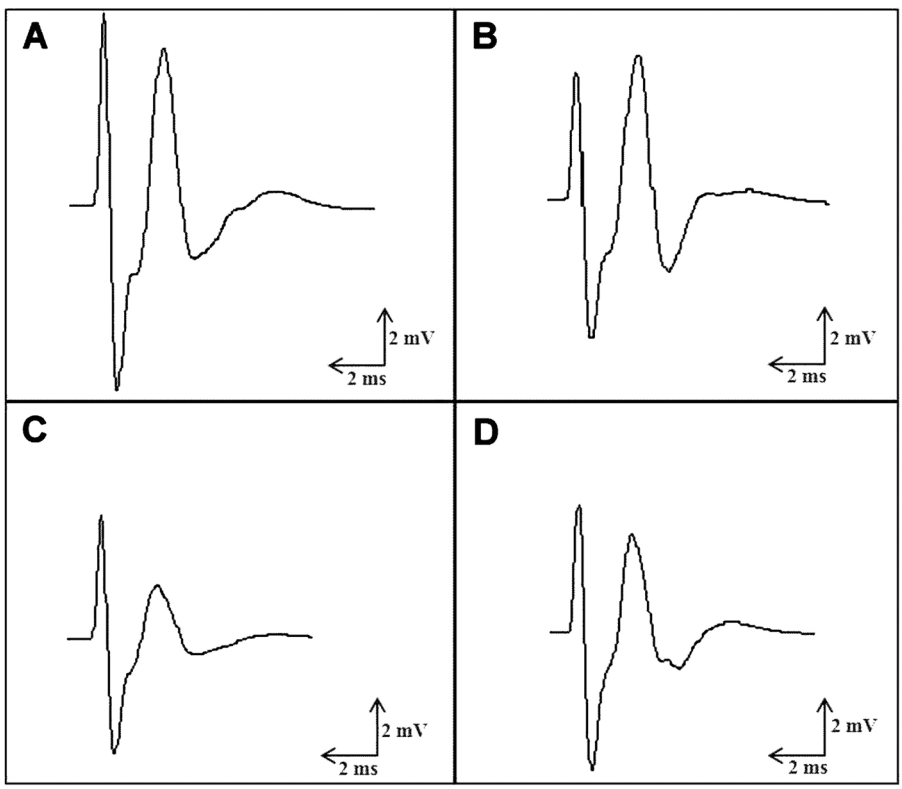


Fig. 4. Recordings of CMAP samples from control group (A), paricalcitol group (B), RF group (C), and RF + paricalcitol group (D).



1521186x, 2018, 8, Downloaded from https://onlinelibrary.wiley.com/doi/10.1002/bem.22149 by University Of British Columbia, Wiley Online Library on [16/10/2026]. See the Terms and Conditions (https://onlinelibrary.wiley.com/terms-and-conditions) on Wiley Online Library for rules of use; OA articles are governed by the applicable Creative Commons License

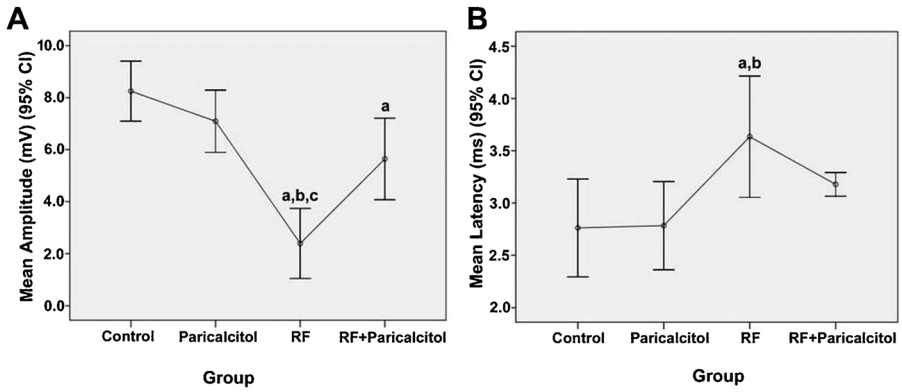


Fig. 5. CMAP amplitude (A) and latency (B) values in control and experimental groups. CI: confidence interval. Error bars represent mean ± standard deviation values. [a]$P < 0.05$ compared with control group; [b]$P < 0.05$ compared with paricalcitol group; [c]$P < 0.05$ compared with RF + paricalcitol group.

group, the amplitude of CMAP was different from the control group ($P < 0.05$) (Fig. 5A).

In the RF group, the latency of action potential was significantly prolonged compared with the control, paricalcitol, and RF + paricalcitol values (Fig. 5B). When the other groups were compared with each other, no significant differences were observed in latency values ($P > 0.05$). Values of mean latency were $2.76 \pm 0.23$, $2.78 \pm 0.$ 21, $3.63 \pm 0.29$, and $3.17 \pm 0.13$ ms in control, paricalcitol, RF, and RF + paricalcitol groups, respectively.

## Biochemical Findings

MDA level and CAT activity for all groups are shown in Table 3. In RF group, the MDA levels significantly increased when compared to control, paricalcitol, and RF + paricalcitol groups ($P < 0.05$). In the RF + paricalcitol group, MDA level was significantly lower than RF group ($P < 0.05$). There was no significant difference between control, paricalcitol, and RF + paricalcitol groups ($P > 0.05$). Mean CAT activity in RF group significantly increased when compared to control, paricalcitol, and RF + paricalcitol groups ($P < 0.05$). In the RF + paricalcitol group, mean CAT activity was significantly higher than the control group ($P < 0.05$) but was significantly lower than RF group ($P < 0.05$). Paricalcitol treatment decreased both MDA level and CAT activity.

## Light Microscopic Evaluation

In the control group and paricalcitol group, myelinated nerve fibers were observed in normal histologic appearance (96.1% and 94.9% of myelinated nerve fibers, respectively) (Fig. 6A and B). Normal and degenerated myelinated nerve fibers were observed in the RF and RF + paricalcitol groups (Fig. 6C and D). The rate of degeneration in myelinated nerve fibers was 68.8% in the RF group and 42.6 % in the RF + paricalcitol groups.

In the RF group, myelin thickness significantly increased and g-ratio significantly decreased compared to those in the control group ($P < 0.05$ and $P < 0.05$, respectively) and paricalcitol group ($P < 0.05$ and $P < 0.05$, respectively). In the RF +

**TABLE 3. Evaluated Biochemical Parameters in Sciatic Nerve**

| Variable | Control | Paricalcitol | RF | RF + Paricalcitol |
|---|---|---|---|---|
| CAT (U/mg protein) | $217.97 \pm 70.49$ | $290.95. \pm 69.29$ | $845.24 \pm 169.60^{*,**,***}$ | $451.52 \pm 160.85^{****}$ |
| MDA (nmol/mg protein) | $128.75 \pm 18.80$ | $103.99 \pm 32.85$ | $238.54 \pm 78.33^{*,**,***}$ | $164.95 \pm 5.51$ |
| Myelin thickness (μm) | $4.29 \pm 1.34$ | $4.17 \pm 1.21$ | $9.64 \pm 2.04^{*,**,***}$ | $7.43 \pm 1.98^{****}$ |
| g-ratio | $0.66 \pm 0.11$ | $0.63 \pm 0.21$ | $0.35 \pm 0.08^{*,**,***}$ | $0.56 \pm 0.10$ |
| Myelin sheath damage grade | $0.10 \pm 0.07$ | $0.12 \pm 0.06$ | $1.47 \pm 0.33^{*,**,***}$ | $0.67 \pm 0.08^{****}$ |
| Axonal damage score | $0.13 \pm 0.08$ | $0.13 \pm 0.07$ | $0.93 \pm 0.39^{*,**,***}$ | $0.41 \pm 0.18^{****}$ |

All data are presented as mean ± SD.
*$P < 0.05$ compared with RF and control groups.
**$P < 0.05$ compared with RF and paricalcitol groups.
***$P < 0.05$ compared with RF and RF + paricalcitol groups.
****$P < 0.05$ compared with RF + paricalcitol and control groups.



1521186x, 2018, 8, Downloaded from https://onlinelibrary.wiley.com/doi/10.1002/bem.22149 by University Of British Columbia, Wiley Online Library on [16/10/2026]. See the Terms and Conditions (https://onlinelibrary.wiley.com/terms-and-conditions) on Wiley Online Library for rules of use; OA articles are governed by the applicable Creative Commons License

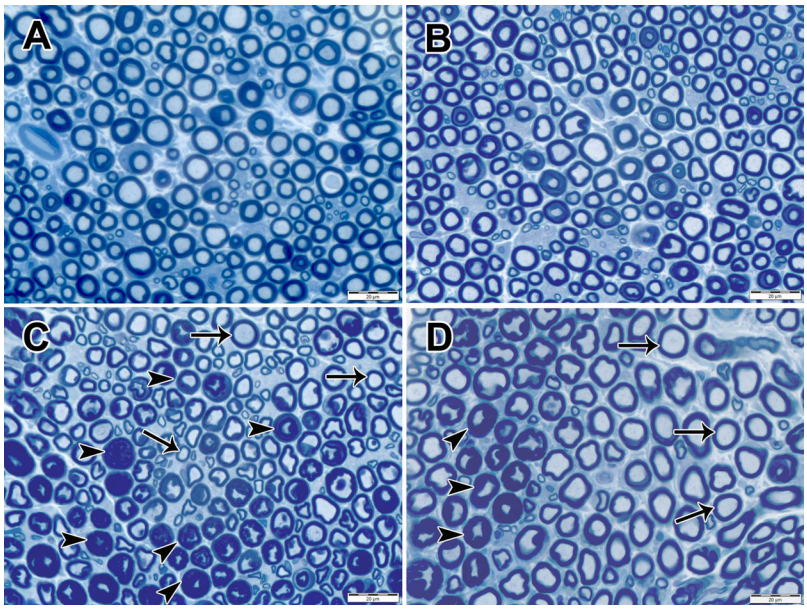


Fig. 6. Light micrographs of myelinated nerve fibers (Toluidine Blue ×400). Normal myelinated nerve fibers are shown in the control group (A) and paricalcitol group (B). Normal myelinated nerve fibers (arrows) and degenerated myelinated nerve fibers (arrowheads) are shown in the RF group (C) and RF + paricalcitol group (D).

paricalcitol group, the myelin thickness significantly decreased and g-ratio significantly increased compared to the RF group ($P < 0.05$ and $P < 0.05$, respectively).

The myelin thickness significantly increased in the RF + paricalcitol group compared to control group and paricalcitol group ($P < 0.05$ and $P < 0.05$, respectively), but no statistically significant difference in g-ratio was seen between control, paricalcitol, and RF + paricalcitol groups (all comparisons $P < 0.05$) (Table 3).

### Transmission Electron Microscopic Evaluation

Normal myelin sheath ultrastructure was observed in the control group and paricalcitol group (Fig. 7A and B). Normal mitochondria ultrastructure and homogeneously dispersed neurotubules and neurofilaments were observed in the axon of myelinated nerve fibers in the control group and paricalcitol group (Figs. 8A and B and 9A and B). In the RF group, degeneration findings were observed in most of the myelinated nerve fibers. In damaged myelinated nerve fibers, disintegration, deformation in the myelin sheaths and myelin ovoids, mitochondria degeneration with swollen cristae, loss of cristae and disruption of membranes, and heterogeneous dispersion of neurotubules and neurofilaments were devoid of neurotubules and neurofilaments in some areas in the axoplasms observed in this group (Fig. 7C, 8C, and 9C). In RF + paricalcitol group, most of the myelinated nerve fibers were found to be in normal ultrastructure. Mitochondrial ultrastructure and organization of neurotubules and neurofilaments in axoplasms were observed as normal in myelinated nerve fibers. However, in some of the myelinated nerve fibers, disintegration in myelin sheaths, swollen mitochondria with disorganized cristae, and disorganized neurotubules and neurofilaments, and myelin ovoid body were also observed in axoplasms in this group (Fig. 7D, 8D, and 9D). The myelin sheath damage grade and axonal damage score significantly increased in the RF group ($1.47 \pm 0.07$ and $0.93 \pm 0.05$, respectively) compared to the control group ($0.10 \pm 0.02$ and $0.13 \pm 0.02$, respectively) and paricalcitol group ($0.12 \pm 0.02$ and $0.14 \pm 0.02$, respectively) (all comparisons $P < 0.05$). In the RF + paricalcitol group, the myelin sheath damage grade and axonal damage score ($0.67 \pm 0.05$ and $0.41 \pm 0.04$, respectively) significantly decreased compared to the RF group, whereas the myelin sheath damage grade and axonal damage score significantly increased than those in the control group and paricalcitol group (all comparisons $P < 0.05$).

## DISCUSSION

The present study investigated alterations in the electrophysiology, biochemistry, and morphology of sciatic nerves exposed to 1,800 MHz RF radiation and



1521186x, 2018, 8, Downloaded from https://onlinelibrary.wiley.com/doi/10.1002/bem.22149 by University Of British Columbia, Wiley Online Library on [16/10/2026]. See the Terms and Conditions (https://onlinelibrary.wiley.com/terms-and-conditions) on Wiley Online Library for rules of use; OA articles are governed by the applicable Creative Commons License

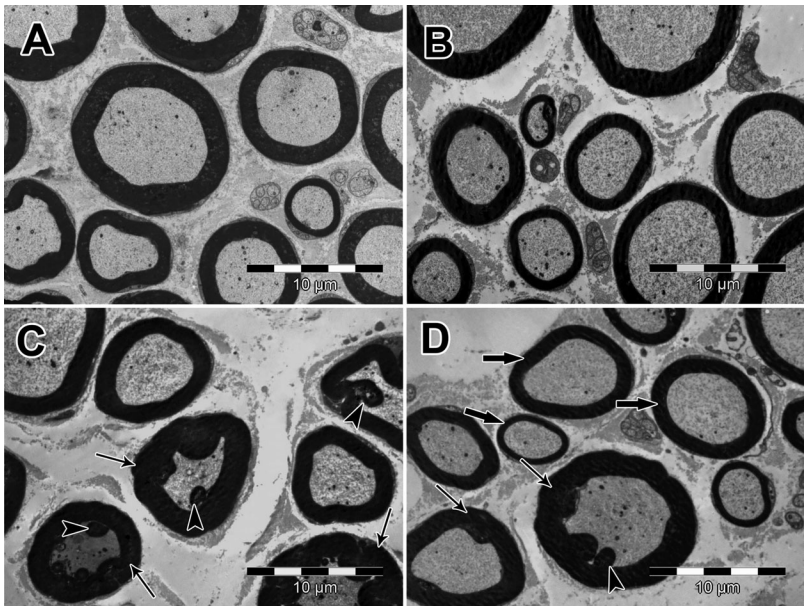


Fig. 7. Transmission electron micrographs of myelin sheaths (×4,000). Ultrastructurally normal myelin sheaths are shown in the control group (A) and paricalcitol group (B). In the RF group (C), degeneration with deformation and thickening of myelin sheaths (thin arrows) and myelin ovoids (arrowheads) in axoplasms, in most of the myelinated nerve fibers, are shown. In the RF + paricalcitol group (D), normal myelin sheaths (thick arrows) and degenerated myelin sheaths with deformation and thickening (thin arrow), and myelin ovoids (arrowheads) in axoplasms in the myelinated nerve fibers are shown.

protective effect of 0.2 μg/kg/day paricalcitol. We observed functional and morphological changes such as neuropathy in rats exposed to RF radiation. Paricalcitol partially ameliorated these changes.

CMAP was recorded to monitor electrical properties of the sciatic nerve. In the RF group, significantly reduced amplitude and prolonged latency were observed in CMAP recordings. When compared to the control group, the reduction in CMAP amplitude was 71% and prolongation of the latency of CMAP was 31.5%. Decreased amplitude and prolonged latency are considered as a sign of neuropathic changes in the peripheral nerves [Aminoff, 1998; Chung et al., 2014]. Paricalcitoltol treatment reduced these ratios for amplitude and latency to 31.6% and 14.8%, respectively, when compared to control group. There are a few studies in the literature that examine the effects of RF radiation on the peripheral nervous system. Acar et al. [2009] studied the thermal effects of 1,900 MHz RF (maximum SAR 3.72 W/k) radiation on facial nerve conduction rate and compound muscle action potentials, and they found that the amplitudes of facial nerve CMAP after RF radiation exposure were significantly smaller than preexposure amplitudes. In another study, Yegin et al. [2017] investigated the effect of mobile phone signals (maximum SAR 5.78 W/kg for 10 g average) on electrical impulse of myelinated nerves and observed that GSM-signal coupling could distort the shape and spectrum of the nerve impulse. Our electrophysiological findings are supported by the results reported by Acar et al. [2009] and Yegin et al. [2017]. The electrophysiological findings presented in our study show different patterns of neuropathy, including axonal and demyelinating neuropathy.

In order to ascertain whether the electrophysiological changes were associated with corresponding alterations in morphological signs of the sciatic nerve, histopathological examinations were also carried out. We found that myelin sheath damage grade and axonal damage score were significantly higher in the sciatic nerve of the RF groups than those of the other groups. In our study, we observed the lowest g-ratio in the RF group and there was a significant difference among the RF group and other groups. Previous studies reported that the prolongation in CMAP latency was due to increased myelin sheath thickness caused by edematous swelling, delamination, and rarefaction in the myelin sheath [Cankayali et al., 2007; Yilmaz et al., 2016]. We also thought that the decrease in CMAP amplitude was due to the decreased g-ratio



1521186x, 2018, 8, Downloaded from https://onlinelibrary.wiley.com/doi/10.1002/bem.22149 by University Of British Columbia, Wiley Online Library on [16/10/2026]. See the Terms and Conditions (https://onlinelibrary.wiley.com/terms-and-conditions) on Wiley Online Library for rules of use; OA articles are governed by the applicable Creative Commons License

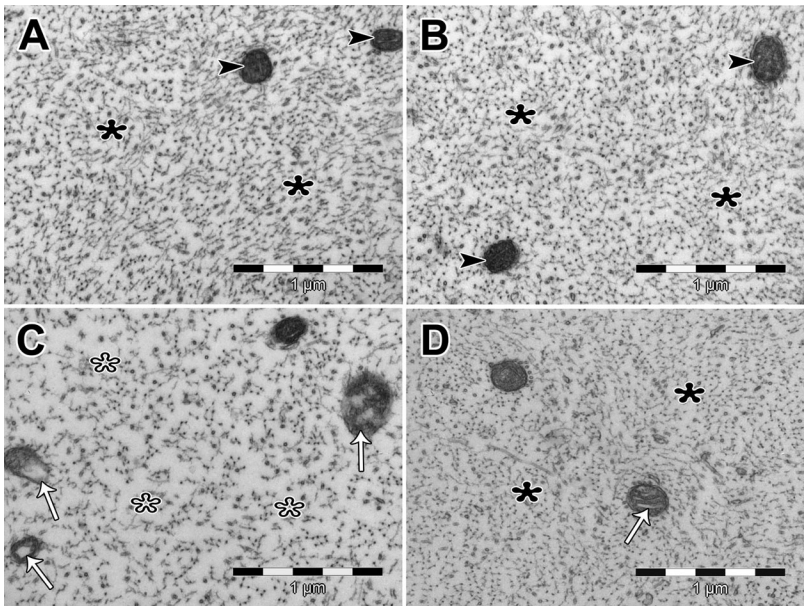


Fig. 8. Transmission electron micrographs of cross sections of myelinated axons (×50,000). Normal mitochondria ultrastructure (arrowheads) and homogeneously dispersed neurotubules and neurofilaments (asterisks) are shown in control group (A) and paricalcitol (B) group. Degenerated mitochondria (white arrows) with swollen cristae, disrupted membranes, and heterogeneously dispersed neurotubules and neurofilaments devoid of neurotubules and neurofilaments in some areas (white asterisks) are shown in the RF group (C). Homogenously dispersed neurotubules and neurofilaments (asterisks) and mitochondria with slightly swollen, disorganized cristae (white arrow) are shown in the RF + paricalcitol group (D).

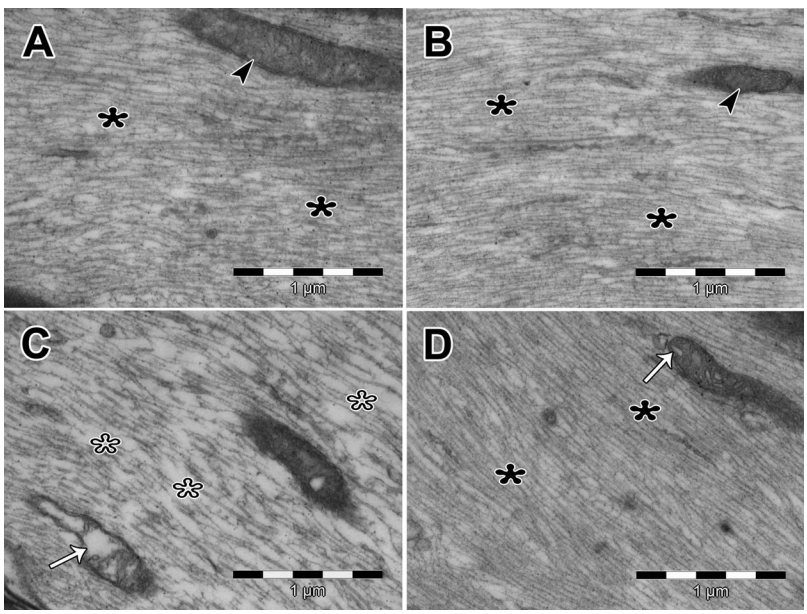


Fig. 9. Transmission electron micrographs of longitudinal sections of myelinated axons (×50,000). Well-aligned neurotubules and neurofilaments (asterisks) and normal mitochondria ultrastructure (arrowheads) are shown in the control group (A) and paricalcitol (B) group. Disorganized neurotubules and neurofilaments and severely degenerated mitochondrion (white arrow) are shown in the RF group (C). Well-aligned neurotubules and neurofilaments (asterisks) and mitochondria with slightly swollen cristae (white arrow) are shown in the RF + paricalcitol group (D).



1521186x, 2018, 8, Downloaded from https://onlinelibrary.wiley.com/doi/10.1002/bem.22149 by University Of British Columbia, Wiley Online Library on [16/10/2026]. See the Terms and Conditions (https://onlinelibrary.wiley.com/terms-and-conditions) on Wiley Online Library for rules of use; OA articles are governed by the applicable Creative Commons License

caused by axonal loss and increase of myelin sheath thickness. Additionally, we observed mitochondrial degeneration with loss of cristae and rupture of inner and outer membranes and disorganization of neurotubules and neurofilaments in the RF group. These histopathological findings support our electrophysiological findings that point to neuropathic changes. There was only one study investigating the histopathological effects of GSM-like RF radiation on peripheral nerves [Kerimoğlu et al., 2018]. Using adolescence rats, Kerimoğlu et al. [2018] examined the effect of 900 MHz RF radiation on sciatic nerve and observed thickening in epineurial layers of sciatic nerves at the light microscopic level. Additionally, it has been reported in some studies that the histological changes in nerve tissue during RF currents can occur due to thermal effects and high intensity electric fields [Podhajsky et al., 2005; Erdine et al., 2009; Tun et al., 2009]. In the literature, many studies have reported that RF radiation increased oxidative stress in different cells and tissue [Moustafa et al., 2001; Ilhan et al., 2004; Ozguner et al., 2005; Meral et al., 2007; Xu et al., 2010]. RF radiation exposure can cause an imbalance between the oxidant-antioxidant process in cells by generating ROS [Dasdag et al., 2008; Sokolovic et al., 2008; Xu et al., 2010; Kesari et al., 2011; İkinci et al., 2016]. In the present study, to determine oxidative stress caused by RF radiation, sciatic nerve MDA levels and CAT activities were measured in all groups. In the RF group, mean MDA level and CAT activity increased by 85.3% and 187%, respectively. Paricalcitol treatment reduced these ratios to 28% and 71%, respectively. MDA, an end product of ROS' attack on membrane lipids, is an important marker of oxidative stress in tissues [Valko et al., 2007]. CAT catalyzes the conversion of hydrogen peroxide to water and molecular oxygen. RF radiation induced an increase in CAT activity which may be explained by its influence on hydrogen peroxide as a substrate that is formed in the process of dismutation of superoxide anion radicals [Ognjanović et al., 2003]. A similar study in the sciatic nerve was performed by Kerimoğlu et al. [2018]. They investigated the effects of exposure to a 900-MHz EMF throughout adolescence on the male rat sciatic nerve and observed an increase in oxidative stress. There are a number of studies that reported the role of oxidative stress in pathophysiology of neuropathy [Naik et al., 2006; Hosseini and Abdollahi, 2013; Areti et al., 2014]. Our electrophysiological, biochemical, and histological findings suggest that 1,800 MHz GSM-like RF radiation has neuropathic changes on the peripheral nerve. This strong damage may be related to the oxidative stress caused by RF radiation.

Previous studies showed the beneficial effects of antioxidants on RF radiation-induced damage [Ilhan et al., 2004; Ozguner et al., 2005; Meral et al., 2007]. In this study, we first showed the effect of paricalcitol on RF radiation-induced neurotoxicity. Paricalcitol is a non-hypercalcemic vitamin D analog that shows similar biological activity as vitamin D. Vitamin D and its non-hypercalcemic analog paricalcitol have pleiotropic and antioxidant effects on cellular homeostasis [Bulut et al., 2016]. In many studies, it was demonstrated that Vitamin D decreases lipid peroxidation and regulations of antioxidant and redox enzyme expression and activation [Wiseman, 1993; Sardar et al., 1996; Gren, 2013]. El-Gohary and Said [2017] demonstrated the protective effect of vitamin D against detrimental effects of RF on the immune system. In the current study, most of the myelinated nerve fibers were found to be in normal ultrastructure in the RF + paricalcitol group. Mitochondrial ultrastructure and organization of neurotubules and neurofilaments were observed as normal in most axoplasms. In the RF + paricalcitol group, the myelin sheath damage grade and axonal damage score significantly decreased compared to the RF group. According to these results, we suggest that Vitamin D supplementation significantly decreased the damage of myelinated nerve fiber in RF radiation-exposed group. This protective effect of Vitamin D is probably due to its regulation of antioxidant defense system function.

Our findings suggest that paricalcitol administration at 0.2 μg/kg/day dose partially ameliorated neurotoxic damage of 1,800 MHz RF radiation. This finding may be related to the applied paricalcitol dose. Full recovery may be achieved at higher doses. We determined the paricalcitol dose according to previous studies in the literature and applied a single dose (0.2 μg/kg/day) [Park et al., 2012; Lee et al., 2016]. The most important limitation of the present study is that the effect of different doses of paricalcitol has not been tested.

## CONCLUSION

In the present study, the effects of 1800 MHz RF radiation on the sciatic nerve were investigated electrophysiologically, biochemically, and histologically. Our findings showed that 1,800 MHz RF radiation could cause neuropathic changes by inducing oxidative stress. Neuropathic damage was partially improved with 0.2 μg/kg/day paricalcitol, non-hypercalcemic vitamin D analog. However, further studies should be performed by applying different



1521186x, 2018, 8, Downloaded from https://onlinelibrary.wiley.com/doi/10.1002/bem.22149 by University Of British Columbia, Wiley Online Library on [16/10/2026]. See the Terms and Conditions (https://onlinelibrary.wiley.com/terms-and-conditions) on Wiley Online Library for rules of use; OA articles are governed by the applicable Creative Commons License

doses to determine the most effective dose of paricalcitol.

## REFERENCES


Acar GO, Yener HM, Savrun FK, Kalkan T, Bayrak I, Enver O. 2009. Thermal effects of mobile phones on facial nerves and surrounding soft tissue. Laryngoscope 119:559–562.

Aebi H. 1984. Catalase in vitro. Methods Enzymol 105:121–126.

Allen S, Bassen H, DInzeo G, Hirata A, Jokela K, Lin J, Mann S, Matthes R, Roy C, Taki M, Wang J, Watanabe S. 2009. Dosimetry of high frequency electromagnetic fields (100 kHz to 300 GHz). In: Vecchia P, Matthes R, Ziegelberger G, Lin J, Saunders R, Swerdlow A, editors. A review. ICNIRP. 16, pp 31. Available from: https://www.emf.ethz.ch/fileadmin/redaktion/public/downloads/4_wissen/externes_material/ICNIRP_effekte_RFReview.pdf

Aminoff MJ. 1998. Nerve conduction studies: basic principles and pathologic correlations. In: Aminoff MJ, editor. Electromyography in Clinical Practice. New York, NY: Churchill Livingstone. pp 113–145.

Areti A, Yerra VG, Naidu V, Kumar A. 2014. Oxidative stress and nerve damage: role in chemotherapy induced peripheral neuropathy. Redox Biol 2:289–295.

Baby NM, Koshy G, Mathew A. 2017. The effect of electromagnetic radiation due to mobile phone use on thyroid function in medical students studying in a medical college in South India. Indian J Endocrinol Metab 21:797–802.

Balci M, Devrim E, Durak I. 2007. Effects of mobile phones on oxidant/antioxidant balance in cornea and lens of rats. Curr Eye Res 32:21–25.

Bortkiewicz A, Gadzicka E, Szymczak W. 2017. Mobile phone use and risk for intracranial tumors and salivary gland tumors-A meta-analy sis. Int J Occup Med Environ Health 30:27–43.

Bulut G, Basbugan Y, Ari E, Erten R, Bektas H, Alp HH, Bayram I. 2016. Paricalcitol may improve oxidative DNA damage on experimental amikacin-induced nephrotoxicity model. Ren Fail 38:751–758.

Cankayali I, Dogan YH, Solak I, Demirag K, Eris O, Demirgoren S, Moral AR. 2007. Neuromuscular deterioration in the early stage of sepsis in rats. Critical Care 11:1–7.

Chapman S, Azizi L, Luo Q, Sitas F. 2016. Has the incidence of brain cancer risen in Australia since the introduction of mobile phones 29 years ago? Cancer Epidemiol 42: 199–205.

Chua NH, Vissers KC, Sluijter ME. 2011. Pulsed radiofrequency treatment in interventional pain management: mechanisms and potential indications-a review. Acta Neurochir (Wien) 153:763–761.

Chung T, Prasad K, Lloyd TE. 2014. Peripheral neuropathy: clinical and electrophysiological considerations. Neuroimaging Clin N Am 24:49–65.

Clemens M, Schenke S, Sutter F, Becker J, Hoeschen C, Zankl M, Weiland T. 2009. Bioelectromagnetic field simulations using high-resolution human anatomy models with the finite integration technique. Frequenz 63:163–167.

Dasdag S, Bilgin HM, Akdag MZ, Celik H, Aksen F. 2008. Effect of long term mobile phone exposure on oxidative and antioxidative process and nitric oxide in rats. Biotechnol Biotechnol Equip 22:992–997.

El-Gohary OA, Said MA. 2017. Effect of electromagnetic waves from mobile phone on immune status of male rats: possible protective role of vitamin D. Can J Physiol Pharmacol 95:151–156.

Erdine S, Bilir A, Cosman ER, Cosman ER, Jr. 2009. Ultrastructural changes in axons following exposure to pulsed radiofrequency fields. Pain Pract 9:407–417.

Gren A. 2013. Effects of vitamin E, C and D supplementation on inflammation and oxidative stress in streptozotocin-induced diabetic mice. Int J Vitam Nutr Res 83:168–175.

Grundler W, Kaiser F, Keilmann F, Walleczek J. 1992. Mechanisms of electromagnetic interaction with cellular systems. Naturwissenschaften 79:551–559.

Hagiwara S, Iwasaka H, Takeshima N, Noguchi T. 2009. Mechanisms of analgesic action of pulsed radiofrequency on adjuvant-induced pain in the rat: roles of descending adrenergic and serotonergic systems. Eur J Pain 13: 249–252.

Hosseini A, Abdollahi M. 2013. Diabetic neuropathy and oxidative stress: therapeutic perspectives. Oxid Med Cell Longev 2013:168039.

Husain K, Ferder L, Mizobuchi M, Finch J, Slatopolsky E. 2009. Combination therapy with paricalcitol and enalapril ameliorates cardiac oxidative injury in uremic rats. Am J Nephrol 29:465–472.

Husain K, Suarez E, Isidro A, Ferder L. 2010. Effects of paricalcitol and enalapril on atherosclerotic injury in mouse aortas. Am J Nephrol 32:296–304.

Hussein S, El-Saba AA, Galal MK. 2016. Biochemical and histological studies on adverse effects of mobile phone radiation on rat's brain. J Chem Neuroanat 78:10–19.

İkinci A, Mercantepe T, Unal D, Erol HS, Şahin A, Aslan A, Baş O, Erdem H, Sönmez OF, Kaya H, Odacı E. 2016. Morphological and antioxidant impairments in the spinal cord of male offspring rats following exposure to a continuous 900MHz electromagnetic field during early and mid-adolescence. J Chem Neuroanat 75:99–104.

Ilhan A, Gurel A, Armutcu F, Kamisli S, Iraz M, Akyol O, Ozen S. 2004. Ginkgo biloba prevents mobile phone-induced oxidative stress in rat brain. Clin Chim Acta 340:153–162.

Kalafatakis F, Bekiaridis-Moschou D, Gkioka E, Tsolaki M. 2017. Mobile phone use for 5 minutes can cause significant memory impairment in humans. Hell J Nucl Med 20: 146–154.

Kaptanoglu E, Palaoglu S, Surucu HS, Hayran M, Beskonakli E. 2002. Ultrastructural scoring of graded acute spinal cord injury in the rat. J Neurosurg 97:49–56.

Kerimoğlu G, Güney C, Ş Ersöz, Odacı E. 2018. A histopathological and biochemical evaluation of oxidative injury in the sciatic nerves of male rats exposed to a continuous 900-megahertz electromagnetic field throughout all periods of adolescence. J Chem Neuroanat 91:1–7.

Kesari KK, Kumar S, Behari J. 2011. 900-MHz microwave radiation promotes oxidation in rat brain. Electromagn Biol Med 30:219–234.

Kim JH, Kim HJ, Yu DH, Kweon HS, Huh YH, Kim HR. 2017. Changes in numbers and size of synaptic vesicles of cortical neurons induced by exposure to 835 MHz radiofrequency-electromagnetic field. PloS ONE 12:e0186416.

Lee AS, Jung YJ, Thanh TN, Lee S, Kim W, Kang KP, Park SK. 2016. Paricalcitol attenuates lipopolysaccharide-induced myocardial inflammation by regulating the NF-κB signaling pathway. Int J Mol Med 37:1023–1029.

Lowry OH, Rosenbrough NJ, Farr AL, Randall RJ. 1951. Protein measurement with the folin phenol reagent. J Biol Chem 193:265–275.




1521186x, 2018, 8, Downloaded from https://onlinelibrary.wiley.com/doi/10.1002/bem.22149 by University Of British Columbia, Wiley Online Library on [16/10/2026]. See the Terms and Conditions (https://onlinelibrary.wiley.com/terms-and-conditions) on Wiley Online Library for rules of use; OA articles are governed by the applicable Creative Commons License

Martin HD, Palmer IJ, Hatem M. 2014. Monopolar radiofrequency use in deep gluteal space endoscopy: sciatic nerve safety and fluid temperature. Arthroscopy 30:60–64.

Meral I, Mert H, Mert N, Deger Y, Yoruk I, Yetkin A, Keskin S. 2007. Effects of 900-MHz electromagnetic field emitted from cellular phone on brain oxidative stress and some vitamin levels of guinea pigs. Brain Res 1169:120–124.

Misek J, Belyaev I, Jakusova V, Tonhajzerova I, Barabas J, Jakus J. 2018. Heart rate variability affected by radiofrequency electromagnetic field in adolescent students. Bioelectromagnetics 39:277–288.

Mohan M, Khaliq F, Panwar A, Vaney N. 2016. Does chronic exposure to mobile phones affect cognition? Funct Neurol 31:47.

Moustafa YM, Moustafa RM, Belacy A, Abou-El-Ela SH, Ali FM. 2001. Effects of acute exposure to the radiofrequency fields of cellular phones on plasma lipid peroxide and antioxidase activities in human erythrocytes. J Pharm Biomed Anal 26:605–608.

Naik AK, Tandan SK, Dudhgaonkar SP, Jadhav SH, Kataria M, Prakash VR, Kumar D. 2006. Role of oxidative stress in pathophysiology of peripheral neuropathy and modulation by N-acetyl-L-cysteine in rats. Eur J Pain 10:573–579.

Narayanan SN, Mohapatra N, John P, Nalini K, Kumar RS, Nayak SB, Bhat PG. 2018. Radiofrequency electromagnetic radiation exposure effects on amygdala morphology, place preference behavior and brain caspase-3 activity in rats. Environ Toxicol Pharmacol 58:220–229.

Niedzielska E, Smaga I, Gawlik M, Moniczewski A, Stankowicz P, Pera J, Filip M. 2016. Oxidative stress in neurodegenerative diseases. Mol Neurobiol 53:4094–4125.

Ognjanović BI, Pavlović SZ, Maletić SD, Zikić RV, Stajn AS, Radojicić RM, Saicić ZS, Petrović VM. 2003. Protective influence of vitamin E on antioxidant defense system in the blood of rats treated with cadmium. Physiol Res 52:563–570.

Oktem F, Ozguner F, Mollaoglu H, Koyu A, Uz E. 2005. Oxidative damage in the kidney induced by 900-MHz-emitted mobile phone: protection by melatonin. Arch Med Res 36:350–355.

Oral B, Guney M, Ozguner F, Karahan N, Mungan T, Comlekci S, Cesur G. 2006. Endometrial apoptosis induced by a 900-MHz mobile phone: preventive effects of vitamins E and C. Adv Ther 23:957–973.

Ozguner F, Altinbas A, Ozaydin M, Dogan A, Vural H, Kisioglu AN, Cesur G, Yildirim NG. 2005. Mobile phone-induced myocardial oxidative stress: protection by a noval antioxidant agent caffeic acid phenethyl ester. Toxicol Ind Health 21:223–230.

Ozguner F, Bardak Y, Comlekci S. 2006. Protective effects of melatonin and caffeic acid phenethyl ester against retinal oxidative stress in long-term use of mobile phone: a comparative study. Mol Cell Biochem 282:83–88.

Park JW, Cho JW, Joo SY, Kim CS, Choi JS, Bae EH, Ma SK, Kim SH, Lee J, Kim SW. 2012. Paricalcitol prevents cisplatin-induced renal injury by suppressing apoptosis and proliferation. Eur J Pharmacol 683:301–309.

Podhajsky RJ, Sekiguchi Y, Kikuchi S, Myers RR. 2005. The histologic effects of pulsed and continuous radiofrequency lesions at 42 degrees C to rat dorsal root ganglion and sciatic nerve. Spine 30:1008–1013.

Prasad M, Kathuria P, Nair P, Kumar A, Prasad K. 2017. Mobile phone use and risk of brain tumours: a systematic review of association between study quality, source of funding, and research outcomes. Neurol Sci 38: 797–810.

Sardar S, Chakrabarty A, Chatterjee M. 1996. Comparative effectiveness of vitamin D3 and vitamin E on peroxidation of lipids and enzymes of the hepatic antioxidant system in Sprague-Dawley rats. Int J Vit Nutr Res 66:39–45.

Sato Y, Kojimahara N, Yamaguchi N. 2017. Analysis of mobile phone use among young patients with brain tumors in Japan. Bioelectromagnetics 38:349–355.

Sırav B, Seyhan N. 2016. Effects of GSM modulated radiofrequency electromagnetic radiation on permeability of blood-brain barrier in male & female rats. J Chem Neuroanat 75:123–127.

Sokolovic D, Djindjic B, Nikolic J, Bjelakovic G, Pavlovic D, Kocic G, Krstic D, Cvetkovic T, Pavlovic V. 2008. Melatonin reduces oxidative stress induced by chronic exposure of microwave radiation from mobile phones in rat brain. J Radiat Res 49:579–586.

Tun K, Cemil B, Gurcay AG, Kaptanoglu E, Sargon MF, Tekdemir I, Comert A, Kanpolat Y. 2009. Ultrastructural evaluation of pulsed radiofrequency and conventional radiofrequency lesions in rat sciatic nerve. Surg Neurol 72:496–500.

Valko M, Leibfritz D, Moncol J, Cronin MT, Mazur M, Telser J. 2007. Free radicals and antioxidants in normal physiological functions and human disease. Int J Biochem Cell Biol 39:44–84.

Wiseman H. 1993. Vitamin D is a membrane antioxidant. Ability to inhibit iron-dependent lipid peroxidation in liposomes compared to cholesterol, ergosterol and tamoxifen and relevance to anticancer action. FEBS Lett 326:285–288.

Xu S, Zhou Z, Zhang L, Yu Z, Zhang W, Wang Y, Wang X, Li M, Chen Y, Chen C, He M, Zhang G, Zhong M. 2010. Exposure to 1800MHz radiofrequency radiation induces oxidative damage to mitochondrial DNA in primary cultured neurons. Brain Res 1311:189–196.

Yagi K. 1998. Simple procedure for specific enzyme of lipid hydroperoxides in serum or plasma. Methods Mol Biol 108:107–110.

Yegin K, Yegin EG, Dasdag S. 2017. Effect of mobile phone signals on electrical impulses of myelinated nerve fibres. J Int Dent Med Res 10:186–192.

Yilmaz M, Aktug H, Oltulu F, Erbas O. 2016. Neuroprotective effects of folic acid on experimental diabetic peripheral neuropathy. Toxicol Ind Health 32:832–840.



1521186x, 2018, 8, Downloaded from https://onlinelibrary.wiley.com/doi/10.1002/bem.22149 by University Of British Columbia, Wiley Online Library on [16/10/2026]. See the Terms and Conditions (https://onlinelibrary.wiley.com/terms-and-conditions) on Wiley Online Library for rules of use; OA articles are governed by the applicable Creative Commons License